AD-A120 318 CALIFORNIA UNIV LOS ANGELES DEPT OF ELECTRICAL ENGI--ETC F/G 20/14
COMPACT MILLIMETER WAVE CYCLOTRON RESONANCE MASER.(U)
AUG 82 N C LUHMANN, D B MCDERMOTT AFOSR-81-0200
UNCLASSIFIED ENG-82-65 AFOSR-TR-82-0866 NL

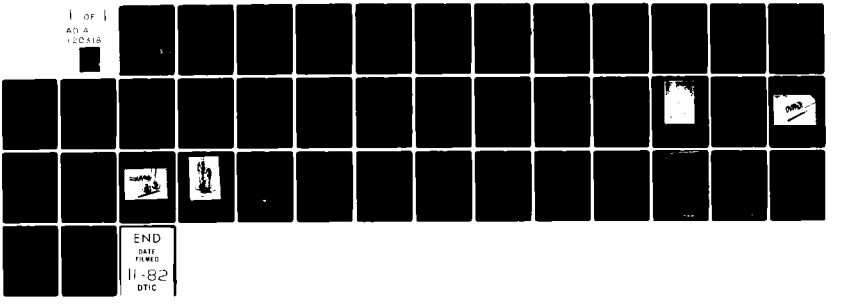

END
DATE FILMED
11-82
DTIC

AFOSR-TR- 82-0866

AUGUST 1982

(3)

PROGRESS REPORT

# COMPACT MILLIMETER WAVE CYCLOTRON RESONANCE MASER

PRINCIPAL INVESTIGATOR: N.C. LUHMANN, JR.
Professor

CO-PRINCIPAL INVESTIGATOR: W.A. PEEBLES
Research Engineer

Research sponsored by the
United States
Air Force Office of Scientific Research
under Grant No. 81-0200

Contract Period: June 15, 1981 - June 15, 1982



Electrical Engineering Department
School of Engineering and Applied Science
University of California
Los Angeles, California 90024

PROGRESS DURING CURRENT GRANT PERIOD

(June 15, 1981 - June 15, 1982)

# I. INTRODUCTION

During the 1981-1982 fiscal year, the experimental efforts have focussed on building the gyrotron chamber and associated apparatus. The system is now operational and measurements have begun. The results have been extremely encouraging. Using only 50 kW of the 200 kW available from our X-band magnetron, the rf accelerator has produced 100 mA, 100-250 keV beams. Millimeter wave measurements have been made. Our second gyrotron cavity, which was designed to be excited by $\sim$ 150 keV beams, has yielded $\sim$ 100 W at 26-46 GHz (3rd-6th cyclotron harmonics), corresponding to 1% electron to output wave energy conversion efficiency. This cavity was designed to be undercoupled due to start-oscillation considerations. Therefore, the efficiency of electron energy into cavity wave power was on the order of 5%. The next cavity to be tested is critically coupled for higher power operation.

Our theoretical activities have also been productive. We have developed a theoretical description of the large-orbit cyclotron harmonic maser which yields encouraging values for device efficiency. Efficiencies as high as 8% have been predicted at millimeter-wavelength operation with a uniform magnetic field. By properly tapering the magnetic field so that the gyrofrequency remains approximately constant as the electrons lose energy this may be increased to 16%. In addition, a small-signal theory of the harmonic gyrotron has been developed which yields the value of beam current necessary for oscillation. This theory, discussed in Section II, has already been verified by experimental measurements, which are outlined in Section III. Though a shorter cavity will have a higher peak efficiency, a long cavity requires less beam current for oscillation. Our 1981-1982 conference attendance and publications are listed in Section V.

## II. THEORETICAL RESULTS

The geometry of the harmonic gyrotron is shown in Fig. 1. The electron beam propagates along a uniform magnetic field through a $TE_{nmp}$ cylindrical cavity for which the effect of the drift tube is neglected. The guiding center of the electrons coincides with the axis of the cavity.

We have examined the large-orbit CRM mechanism in a treatment similar to that utilized by Sprangle and Drobot[1] in treating the nonlinear saturation of the gyrotron. We find that the equation describing electron-to-wave energy transfer for the interaction of a large-orbit electron beam with a $TE_{n1}$ waveguide mode is essentially equivalent to that for the conventional small-orbit interaction with the $TE_{n1}$ mode. The rate of change of the electron energy is governed by the equation.

$$\begin{aligned} mc^2 \dot{\gamma} &= e\, E_\phi(t)\, V_\phi(t) \\ &= -e(E_\phi \sin n\phi \cos \omega t)\, v_\perp \end{aligned} \qquad (1)$$

For simplicity of analysis we have assumed that the wave azimuthal electric field of the $TE_{n1}$ mode evaluated at the position of the beam is sufficiently weak that the axi-centered electron velocity $v_\perp$ varies slowly and can be approximated by its initial value. The electron gyrational phase angle is determined by the equation,

$$\dot{\phi} = \frac{eB}{mc\gamma} = \Omega_c \qquad (2)$$

Equations (1) and (2) can be solved by the method of iteration. The average energy change of the electrons (i.e., integration over initial phase angle to second order is found to be:

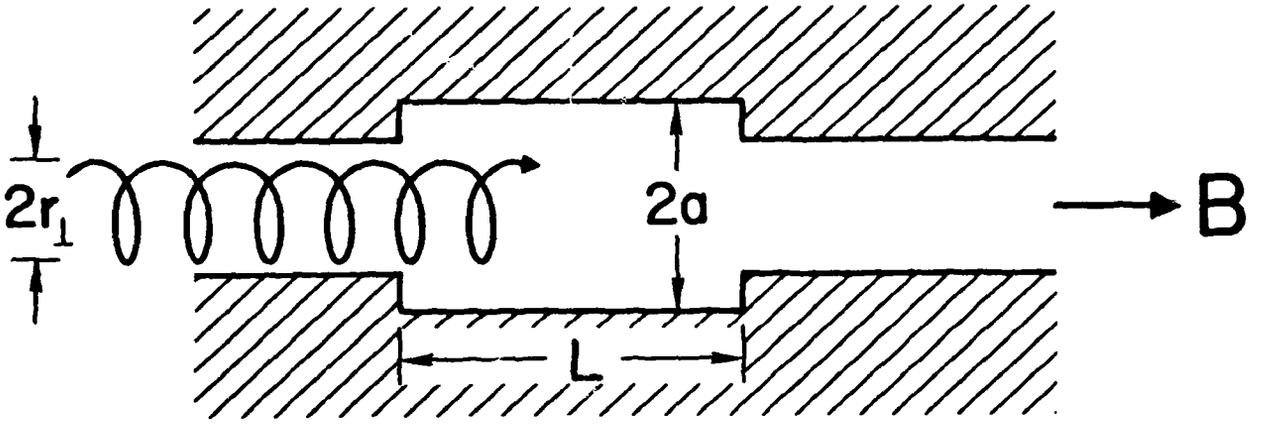


Figure 1. Cross-sectional view of the harmonic gyrotron tube. The Larmor radius $r_\perp$ is equal to $v_\perp / \Omega_c$.

$$\Delta\gamma mc^2 = \frac{ne^2 v_\perp^2 E_\phi^2 \Omega_{co}^2 \tau^3}{16\ \gamma_o mc^2} \sin[(\omega - n\ \Omega_{co})\tau] \qquad (3)$$

where $\tau$ represents the duration of the interaction, $\tau = L/v_{\parallel}$, $v_{\parallel}$ represents the longitudinal velocity, $\Omega_{co} = eB/mc\gamma_o$, and $\omega$ equals the wave frequency. The energy lost by the electrons manifests itself as energy added to the wave. Equation (3) with $n = 1$ is the same equation describing energy transfer in the conventional small-orbit gyrotron.[2] Therefore, this harmonic gyrotron is not inherently a low efficiency interaction.

The efficiency of the device is found by studying the functional dependence of Equation (3). An electron which initially satisfies $(\omega - n\,\Omega_c) > 0$ can continue to lose energy to the wave until $(\omega - n\,\Omega_c) = 0$. Since $\omega$ is fixed by the narrow response width of the resonator, and since $v_{\parallel}$ is constant if the wave-particle interaction only extracts energy from the perpendicular electron motion, we have

$$\Delta\left[(\omega - n\ \Omega_c)\frac{L}{v_{\parallel}}\right] \approx \frac{\Delta\gamma}{\gamma}\frac{\omega L}{v_{\parallel}} \qquad (4)$$

If the device is operated as an oscillator, the initial condition should be such that $(\omega - n\,\Omega_{co})\frac{L}{v_{\parallel}} = \pi/2$ for minimum start oscillation current. The maximum $\Delta\gamma/\gamma$, given by Equation (5) is

$$\left(\frac{\Delta\gamma}{\gamma}\right)_{max} = \frac{v_{\parallel}}{\omega L}\ \frac{\pi}{2} \qquad (5)$$

Using the experimental conditions associated with Jory's device, from Equation (5) we would expect a $(\Delta\gamma/\gamma)$ of 0.75% or 2.0% efficiency (efficiency $\simeq \Delta\gamma/\gamma - 1$), which nearly coincides with his actual operating efficiency — an overall efficiency of 0.4% included the energy lost in the accelerator. Optimization of Jory's device will involve minimizing the interaction time, or including magnetic field tapering so that $\Omega_c$ remains approximately

constant as the electrons lose energy. Either improvement will imply increasing the beam current to compensate for non-optimum start conditions.

Equations (1) and (2) have also been solved numerically. Twenty electrons with different initial phase values are followed in a frame rotating with the initial beam angular velocity. The average $\gamma$ resulting from the CRM interaction is plotted in Figure 2 for parameters that correspond to a $\gamma_o$ = 1.6, $v_{11}$ = 0.3 c beam propagating through a 1 cm long, 140 GHz resonator. The maximum efficiency, which occurs at $n\,\Omega_{co} = 0.95\,\omega$, is $\simeq 8\%$. The development of phase bunching for these twenty electrons as they propagate through the CRM interaction cavity is shown in Figure 3(a). The beam becomes strongly bunched half way through the cavity around a phase point which will lose energy to the wave. During the interaction thirteen electrons lose energy to the wave and seven gain energy from the wave. Wave trapping of electrons is evident by the end of the interaction.

Simulations have also been performed with the inclusion of a spatially decreasing magnetic field. An efficiency equal to 16% has been obtained by a 4% linear taper of the field for the same parameters associated with Figures 2 and 3(a) except for an increase in field strength consistent with higher power operation. The electron positions in phase space for this simulation are shown in Figure 3(b).

The previous results were obtained from a one-dimensional theory. An important refinement to the analysis is the development of a full three-dimensional theory. If the radial dependence of the interaction is included, then we will find important new effects. As the electrons lose energy, their Larmor radii decrease and they eventually shrink away from interaction with the whispering gallery modes. In the presence of a uniform magnetic field this effect will yield another upper limit on $\Delta\gamma$, which is given by

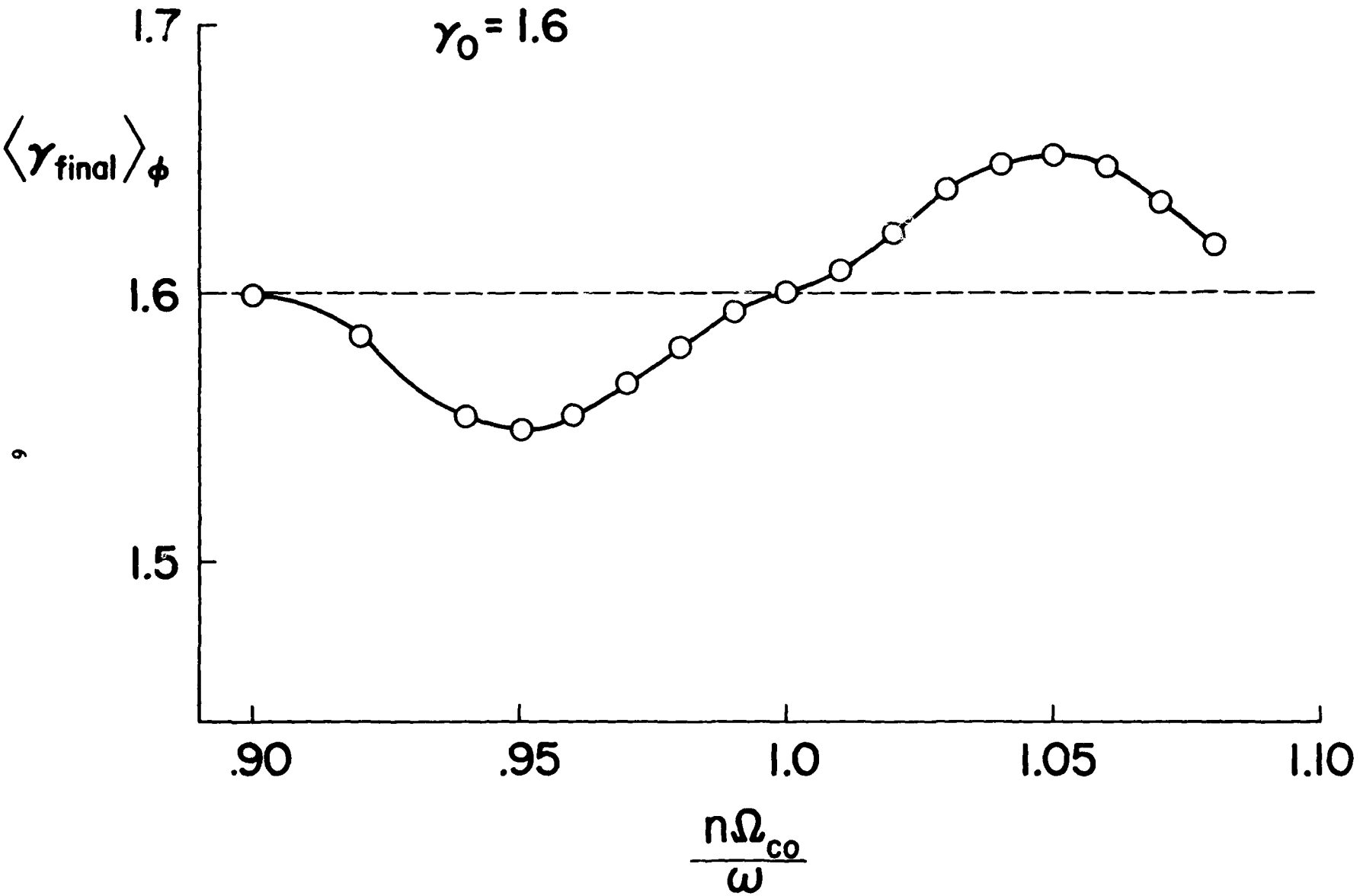


Figure 2. Simulation results of the average electron $\gamma$ after interaction with a $TE_{n11}$ cavity mode as a function of the mismatch ratio $\gamma = (1 - (v_z/c)^2)^{-1/2}$.

$\Delta\gamma/\gamma \approx \delta/r_\perp$, where $r_\perp$ denotes the initial Larmor radius of the beam and $\delta$ represents the width of the $J_n(q_{n1}\, r/a)$ Bessel function ($q_{n1}$ is the first zero of $J_n'(x)$ and a is the cavity radius). For an interaction with a large azimuthal mode number the resultant $\Delta\gamma/\gamma$ can be quite low. However, by tapering the magnetic field we can avoid this effect. Keeping $\Omega_c$ = constant during the interaction for a high - $\gamma$ electron beam is essentially equivalent to holding the Larmor radius constant.

We promised in our grant renewal proposal for the 1982-1983 fiscal year that we would examine theoretically the large-orbit CRM harmonic mechanism in a linearized treatment similar to that utilized by Hirschfield, Bernstein and Wachtel,[3] in describing the conventional gyrotron interaction. We have undertaken the analysis ahead of schedule and finished it during the 1981-1982 fiscal year. We find that the equation describing the interaction of an axis-encircling electron beam with a non-axisymmetric cavity mode is essentially equivalent to that for the conventional small-orbit interaction except that the resonance condition is shifted in favor of much weaker magnetic fields. Therefore, this mechanism is potentially a high efficiency interaction. In order to determine the start oscillation condition for the interaction, we have solved for the power transfer $P = \int d\underset{\sim}{x}\, \underset{\sim}{J}\cdot\underset{\sim}{E}$ between the electrons and the wave, where $\underset{\sim}{J} = -e\int \partial\underset{\sim}{v}\, f_1(\underset{\sim}{x},\underset{\sim}{v},t)$. Here $f_1(\underset{\sim}{x},\underset{\sim}{v},t)$ is the first order perturbed electron distribution function in response to a small amplitude cavity wave. The component of the wave which interacts most strongly with the electrons is the azimuthal electric field, which is given by

$$E_\phi = E_o J_n'\left(\frac{q_{nm} r}{a}\right) \sin(k_{\parallel} z) \sin(n\phi - \omega t) \tag{6}$$

Near the harmonic resonance, where $\omega/n \approx \Omega_c$, the power transfer from the $TE_{n11}$ wave into the electron beam of current I is given in mks units by

$$P = \frac{eIE_o^2 L^2}{mc^2\pi^2\beta_{\parallel}^2}\left[J_n'(n\beta_\perp)\right]^2 R(x) \tag{7}$$

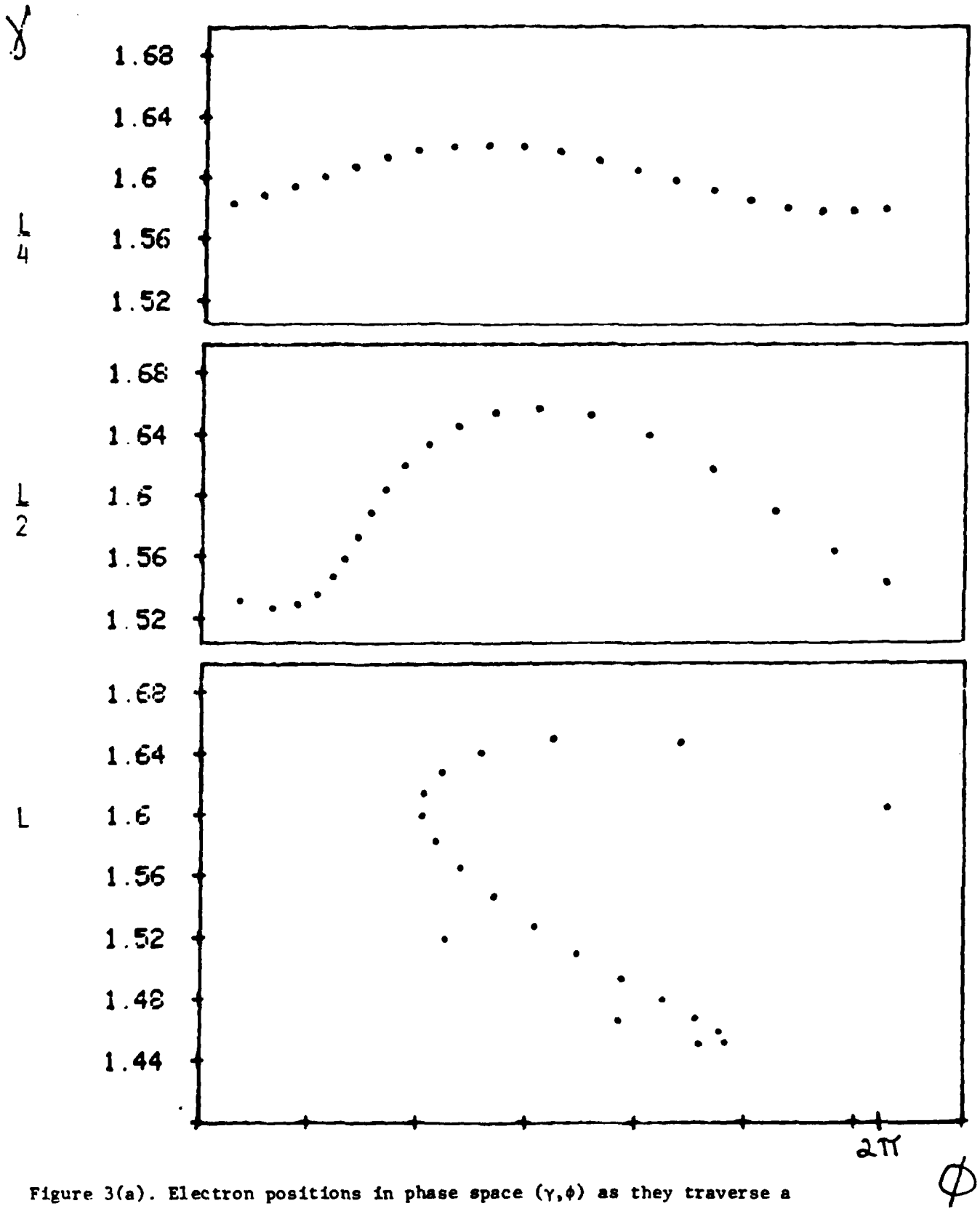


Figure 3(a). Electron positions in phase space $(\gamma,\phi)$ as they traverse a cavity of length L excited by the $TE_{n11}$ mode.

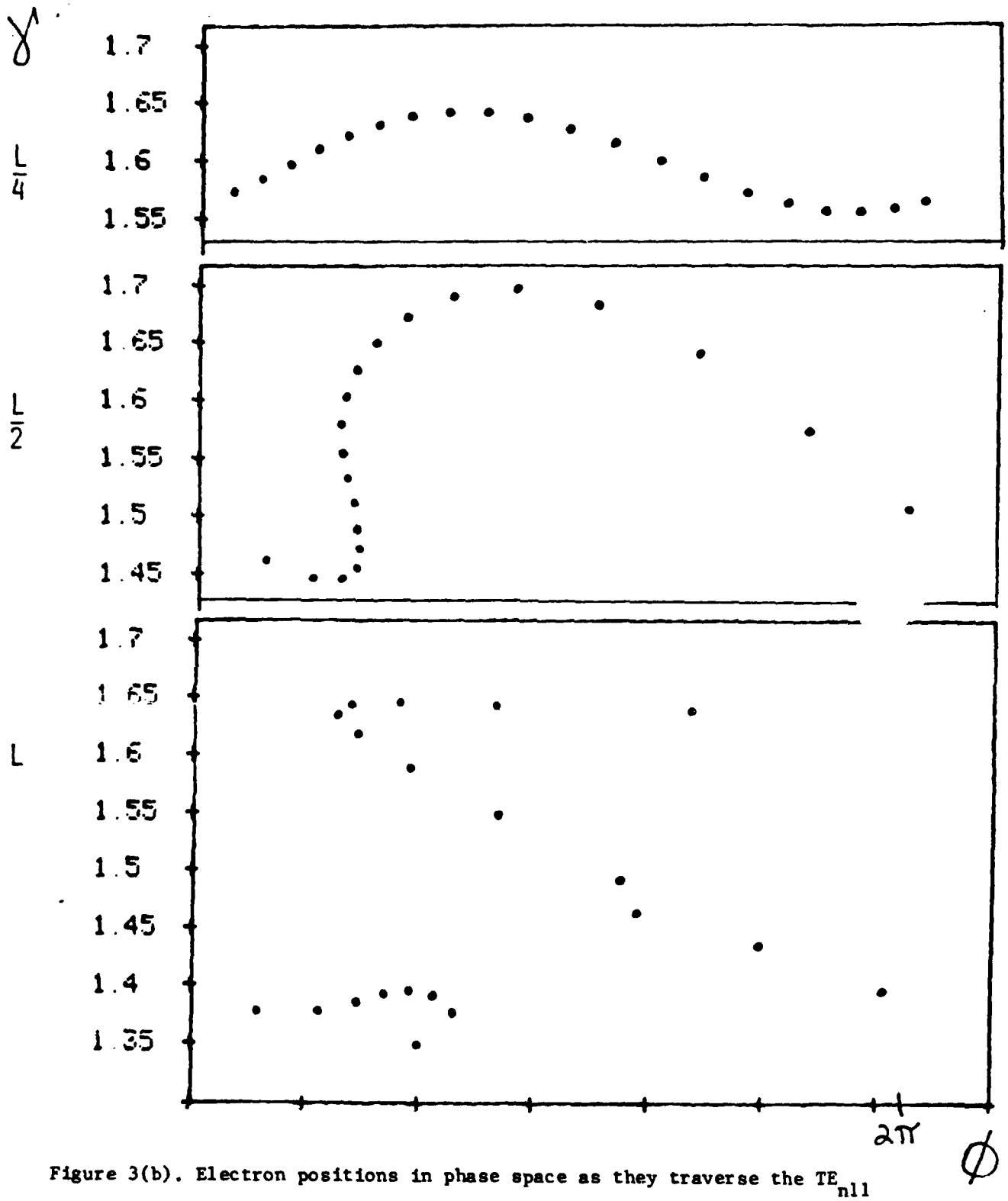


Figure 3(b). Electron positions in phase space as they traverse the $TE_{n11}$ mode; the magnetic field decreases by 4% over the length of the cavity.

where $\beta_{\parallel} = v_{\parallel}/c$ and $\beta_{\perp} = v_{\perp}/c$. The response function R(x) is a complicated function of the electron velocity and the experimental parameters and is plotted in Fig. 4 for two values of cavity length-to-radius ratio (L/a = 2 and 6) and several values of $\beta_{\perp}$ for $TE_{811}$ interaction. For large $\beta_{\perp}$, R(x) is negative, which indicates electron energy loss, for the entire range $0 < x < 3$. Not only does $\beta_{\perp}$ measure the free energy available for interaction but it also measures the filling factor. An increase in $\beta_{\perp}$ will enlarge the beam and radially place the electrons closer to the maximum of the "whispering-gallery" mode.

The effect of the cavity magnetic field upon the energy transfer has been retained in the analysis. The magnetic field bunching, which is in the axial direction, has been shown[4] to compete with the electric field bunching. Azimuthal bunching dominates if $\omega/k_{\parallel}c > 1$ (fast wave interaction) and axial bunching dominates if $\omega/k_{\parallel}c < 1$ (slow wave interaction). The former is well satisfied for the harmonic gyrotron devices that have been built at Varian and at UCLA.

Another competing process, which is especially important for high n interactions, has been included in the derivation. Its effect is proportional to $J_n''(n\beta_{\perp})$ and is due to the dependence of the electron Larmor radius on energy and acts to quench the interaction. If the Larmor radius of the beam is initially smaller than the radius corresponding to the maximum of the $J_n(q_{nm}r/a)$ Bessel function, which we denote by $r_{nm}$, then electrons which gain energy from the cavity wave spiral outwards toward $r_{nm}$ and the interaction increases. As time progresses they gain energy at a faster rate. The interaction decreases in time for electrons which are initially phased so that they lose energy. They progressively lose energy at a slower rate. The beam as a whole will therefore gain energy from the wave. The energy transfer of this mechanism is strongest for resonance where $\omega = n\Omega_c$.

In order to achieve steady-state oscillation the power emitted by the

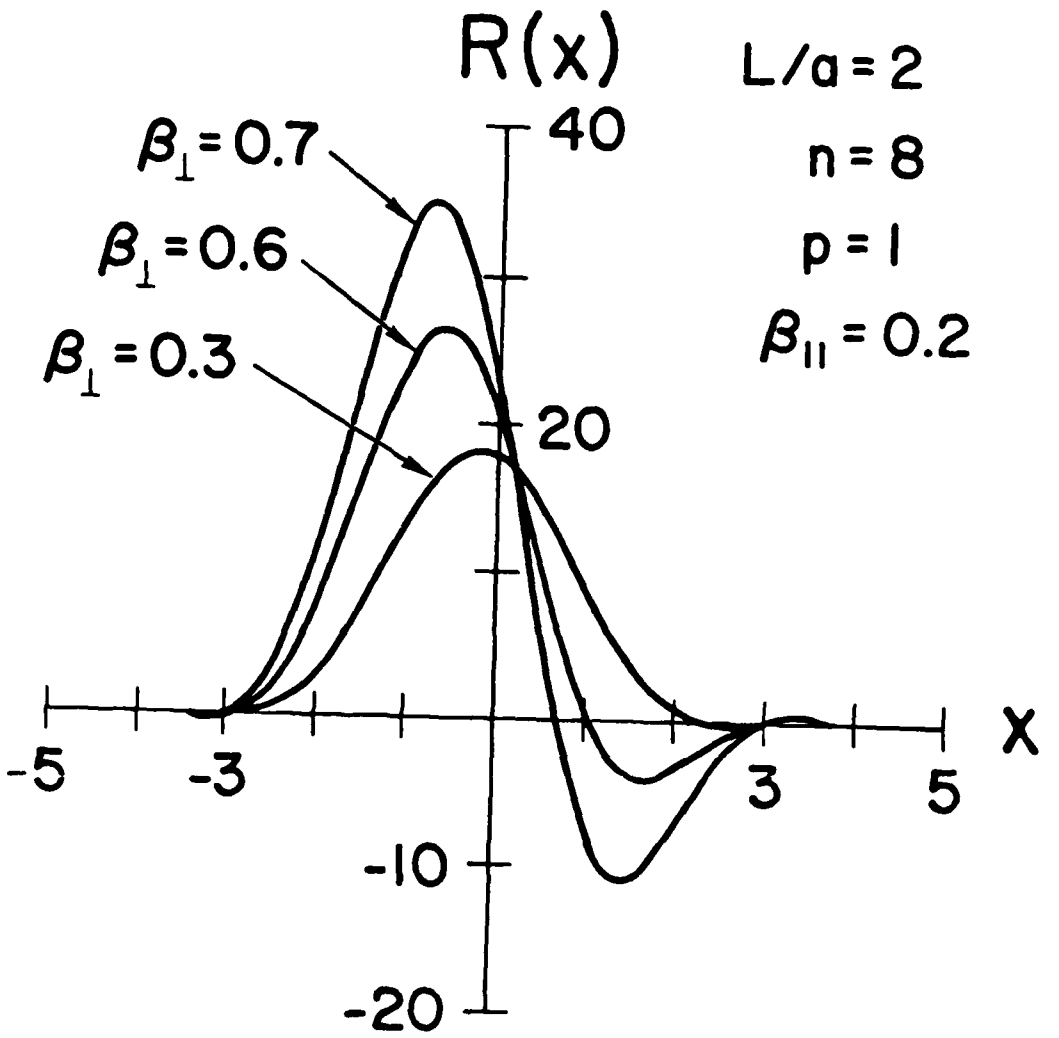


Figure 4(a). Response function for several values of $\beta_\perp$ in a $TE_{811}$ eighth harmonic interaction with the cavity aspect ratio, L/a=2. The electron beam loses energy to the field when R(x) is negative.

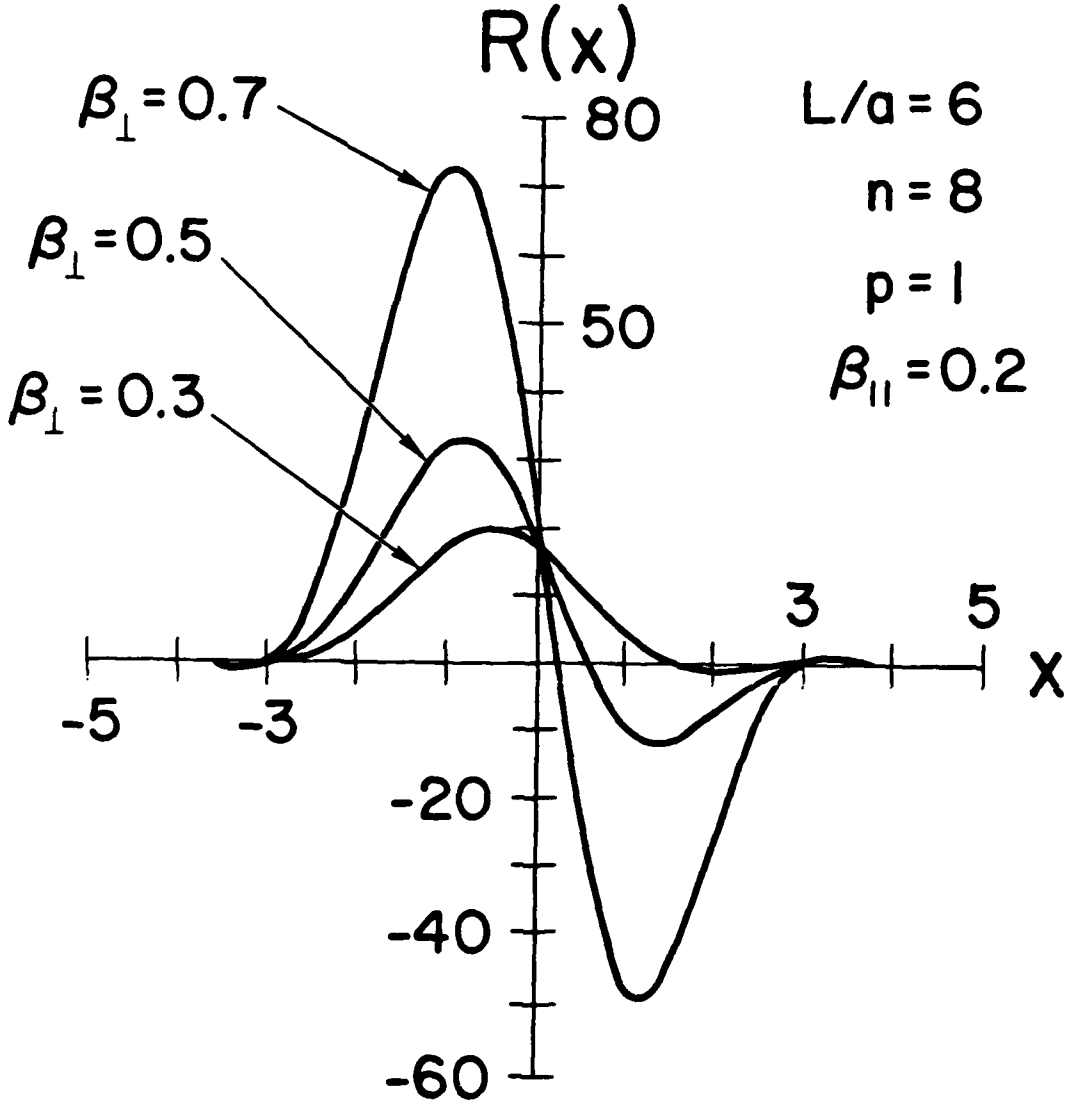


Figure 4(b). Response function for several values of $\beta_\perp$ in a $TE_{811}$ eighth harmonic interaction with the cavity aspect ratio, L/a=6. The electron beam loses energy to the field when R(x) is negative.

electrons must exceed the losses. The dissipated power is simply given by $P_o = \omega U_o/Q_L$ where $U_o$ is the cavity stored energy and $Q_L$ is the loaded quality factor. We have obtained an expression for the required start-oscillation current $I_s$ for a general $TE_{nmp}$ interaction.

$$I_s = \left(\frac{I_A}{16\, Q_L}\right)\left(\frac{\omega}{ck_\perp}\right)(p\pi)^3\left(\frac{a}{L}\right)^2\beta_\parallel^{\,2}\, F_{nm}(\beta_\perp)^{-1}\, R(x)^{-1} \tag{8}$$

where $I_A$ is the Alfven current given by $I_A = 4\pi\varepsilon_o mc^3/e \approx 17$ kA. $F_{nm}(\beta_\perp)$, which represents the filling factor of the beam with the electromagnetic mode, is given by

$$F_{nm}(\beta_\perp) = \left(1 - \frac{n^2}{q^2_{nm}}\right)^{-1}\left[\frac{J_n'(n\beta_\perp)}{J_n(q_{nm})}\right]^2 \tag{9}$$

and plotted in Fig. 5 for several values of n for p=1. The field strength of the $TE_{n11}$ (n>>1) mode peaks near the wall and falls off quickly toward the center.

The start-oscillation current is essentially proportional to $L^{-2}\beta_\parallel^{\,3}$. To maximize the interaction and thereby minimize $I_s$, the energetic electrons should pass slowly through a long cavity. In Fig. 6(a) the start oscillation current as determined by Eq.(8) is shown as a function of magnetic field for the set of parameters, $Q_L \approx 2000$, $\beta_\parallel = 0.15$, $\beta_\perp = 0.75$, $L/a = 6.28$, and $a = 0.438$ cm, which have been chosen to yield 185.5 GHz output. The advantages of this harmonic interaction are apparent. Only 120 mA is required for oscillation; furthermore, the solenoid field strength is less than 7 kG. As shown in Fig. 6(b) by increasing $\beta_\perp$ to 0.85 so that the electrons orbit closer to the mode maximum, $I_s$ can be further reduced to 10 mA. However, the magnetic field must then be increased to 8.7 kG to maintain electron-wave synchronism. The start oscillation condition for interaction with a p=2 mode is eight times larger than for the $TE_{n11}$ interaction.

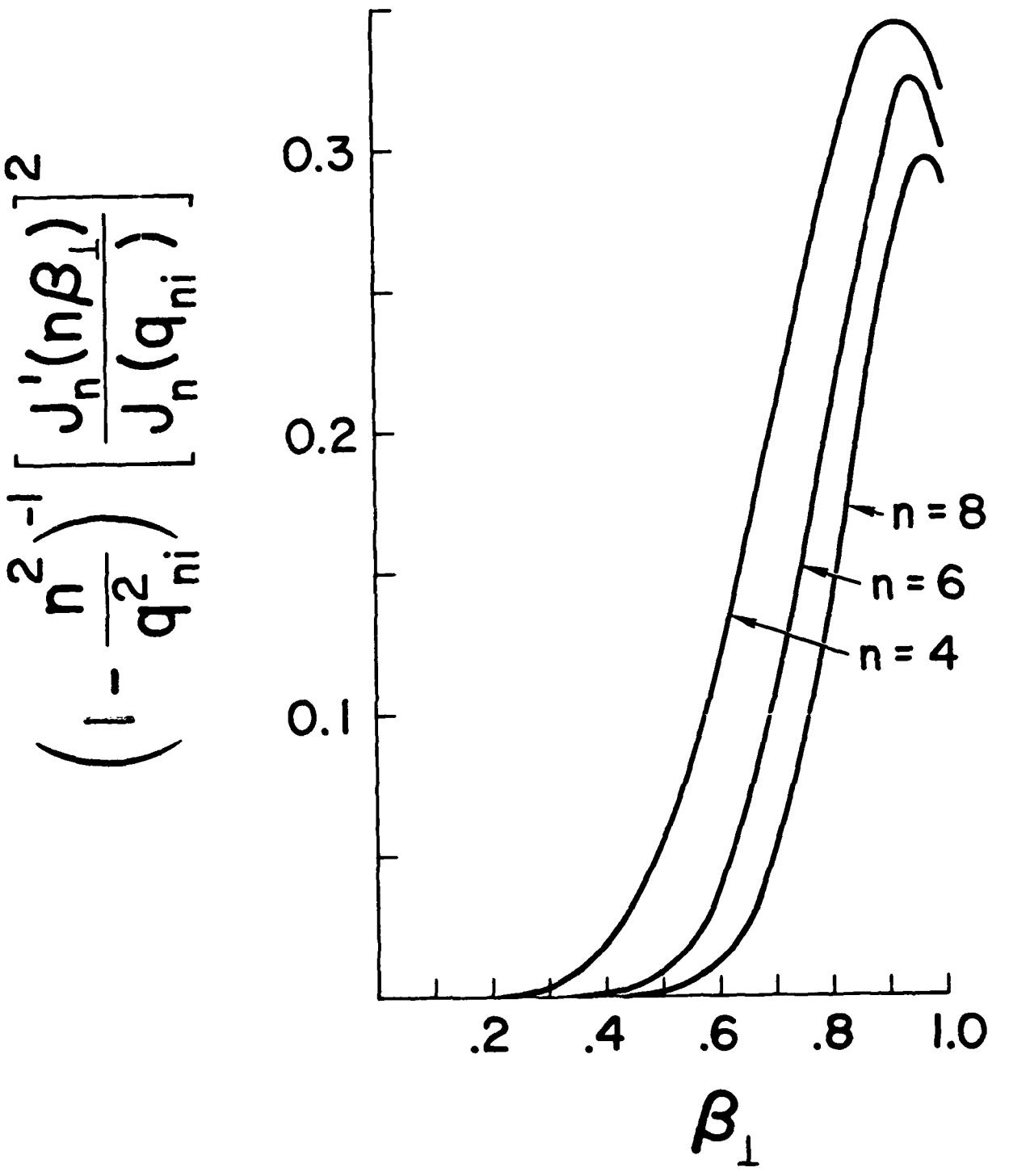


Figure 5. The filling factor as a function of $\beta_\perp$ . It is assumed that $n\Omega_c \approx \omega$.

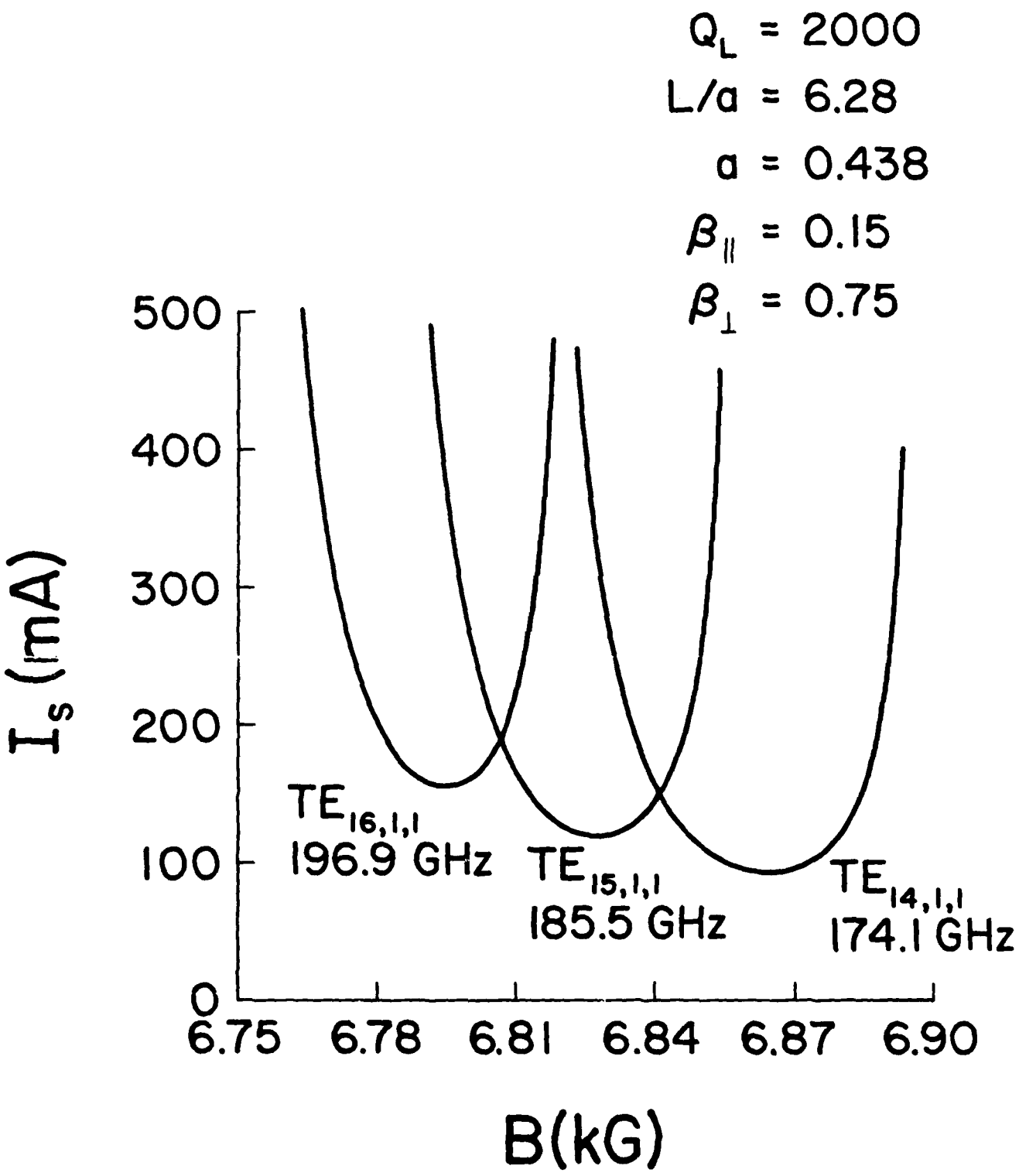


Figure 6(a). Start-oscillation current for three harmonic interactions (n=14, 15, 16) as a function of magnetic field for $\beta_{\perp}$ =0.75.

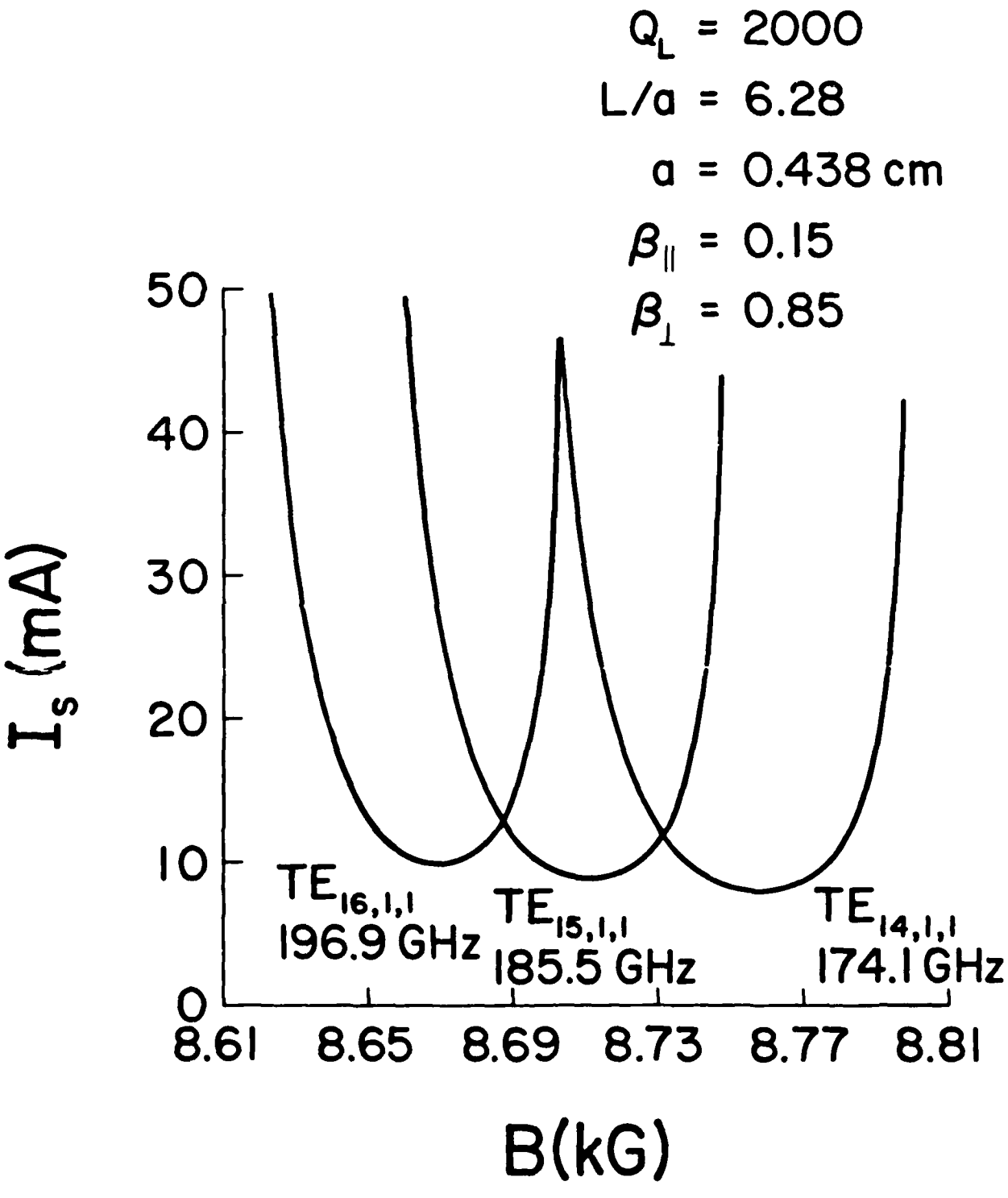


Figure 6(b). Start-oscillation current for three harmonic interactions (n=14, 15, 16) as a function of magnetic field for $\beta_{\perp}$ =0.85.

## III. Experimental Apparatus and Data

A test stand for the UCLA Cyclotron Resonance Maser has been constructed (Fig. 7). The accelerator, millimeter-resonator cavities and coupling structure are mounted on a flange and submerged in a vacuum chamber. Such an arrangement allows great flexibility, especially for quick modification of cavity structures. A combination of $LN_2$ cold-trapped mechanical and absorption pumps brings the pressure down to $\sim 10^{-3}$ Torr. With a two stage ion pump consisting of a 20 ℓ/s starter and a 80 ℓ/s Vacion pump, pressures of $9 \times 10^{-8}$ Torr have been regularly achieved. Ti-sublimation then takes the system down into the $10^{-9}$ range. A large 6-arm cross atop the device provides access for additional vacuum ports and beam diagnostics, which include 1) a quartz glass window for optical pyrometry during cathode activation and electron beam imaging on uranium glass, and 2) a differentially-pumped moveable electron collector. This probe is used for beam position identification and as a thin foil target for x-ray Bremstrahlung radiation detection.

The solenoid consists of two coils placed approximately in a Helmholtz configuration with the bore axis pointing vertically. A 0.9 kA dc power supply provides a magnetic field of up to 6 kG which allows the use of many different accelerator drivers, including an operational 15-17 GHz, 150 kW long pulse TWT amplifier. The present system, however, was chosen to operate at 9.2 GHz where several tunable magnetron sources provide power ranging from 10 kW to 250 kW. R.F. vacuum windows serve as a transition between the X-band and the reduced height guide used for coupling to the accelerator cavity.

UCLA CYCLOTRON RESONANCE MASER

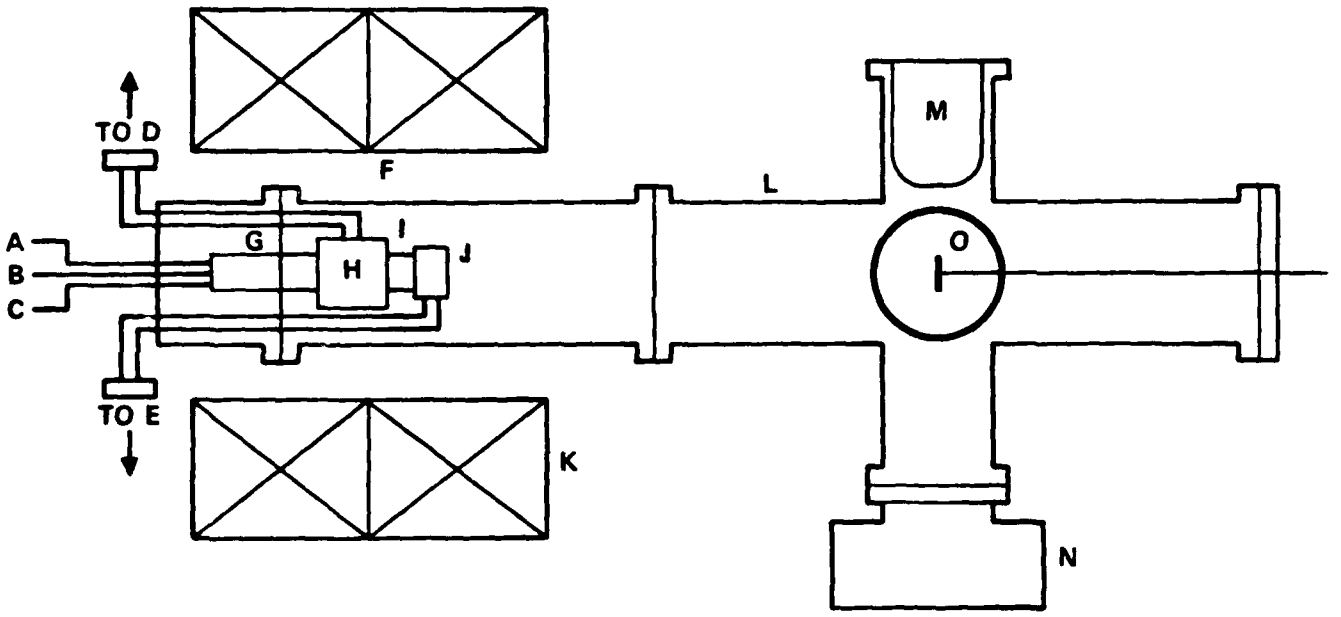


A HEATER/CATHODE BIAS
B HEATER RETURN
C ANODE BIAS
D MAGNETRON rf. ACCELERATOR DRIVE
E HI FREQ. OUTPUT DETECTION
F VACUUM VESSEL
G ELECTRON GUN
H ACCELERATOR CAVITY ($TE_{111}$)
I DRIFT TUBE
J HI FREQ. INTERACTION CAVITY ($TE_{n11}$)
K MAGNET (SOLENOID)
L 6 - ARM CROSS { BEAM DIAGNOSTIC ACCESS, TI - SUB PUMP, ION PUMP, VACSORB, ROUGHING } NOT PICTURED
M $LN_2$ COLD FINGER
N AUXILIARY ION PUMP
O MOVABLE COLLECTOR

Figure 7. Schematic of the vacuum system used in the UCLA Cyclotron Harmonic Maser.

Computer modeling of the magnet coils showed that the magnetic field on axis was smooth to within 1% over the region of interest. Figure 8 shows a computer generated plot of the axial magnetic field strength as a function of axial distance. Actual Hall effect probe measurements of the field are included. The small difference between the simulation and the date is due to the choice of solenoid model where, to minimize date input time, a reduced number of current elements were used and compensated by a correspondingly higher absolute current.

The electron gun (Fig. 9) used in this experiment is a Semicon dispenser cathode with a gridded mesh anode. At 1100°C and 2.0 kV diode voltage, it is capable of delivering 200 mA of current within a 0.3 cm diameter.

Accelerated beam energy measurements are obtained from x-ray pulse height analysis and beam imaging on uranium glass. A $S_2T_{35}$ Harshaw Chemical Co. Thalium-doped Sodium-Iodide scintillation crystal converts x-ray energy to visible light. The resultant photons then impinge on a 7265 photomultiplier tube. The cascaded current is displayed on an oscilloscope across an appropriate load. The scintillator-photomultiplier unit is calibrated with radioactive samples (i.e. $C_s^{137}$).

Another technique for determining the electron energy is to let the beam intersect with a uranium glass plate. The resultant fluorescent image then gives a direct reading of the electron Larmor radius from which the transverse energy can be derived. Since the longitudinal energy is relatively small, we are effectively measuring the total electron energy. A sample view of the electron ring is shown in Fig. 10. An interesting observation is that the thickness of the output ring is equal to the thickness of the initial electron beam.

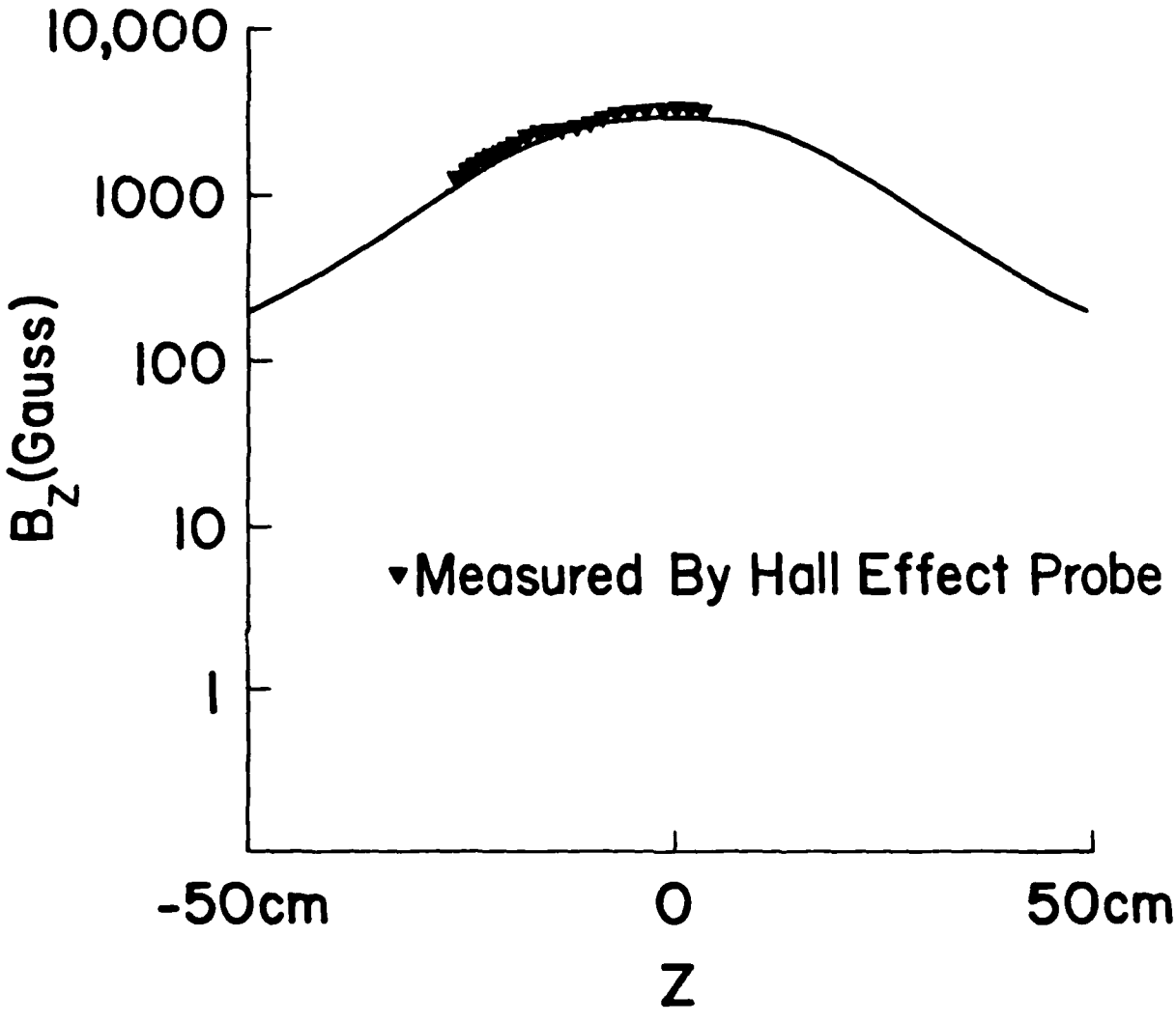


Figure 8. The longitudinal component of the UCLA CRM solenoid magnetic field generated by a computer program and verified by a Hall effect probe.

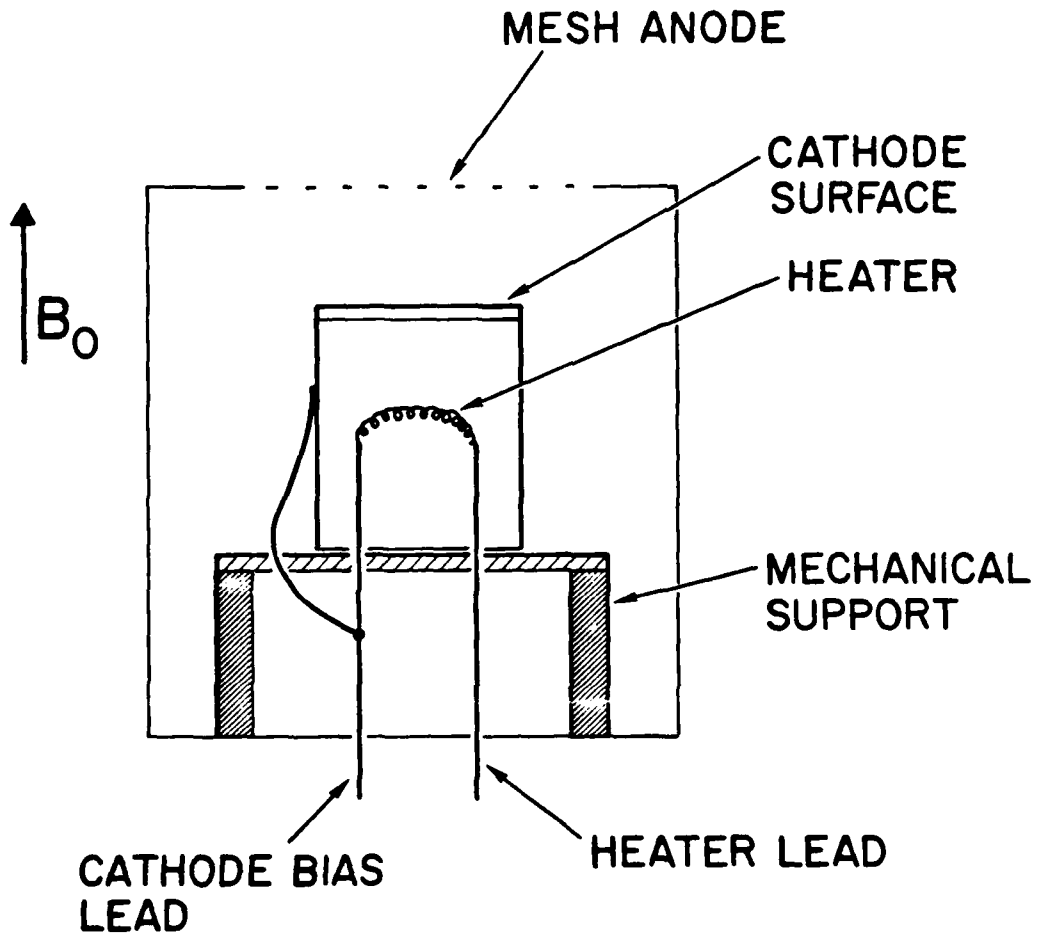


Figure 9. Schematic of the electron gun.

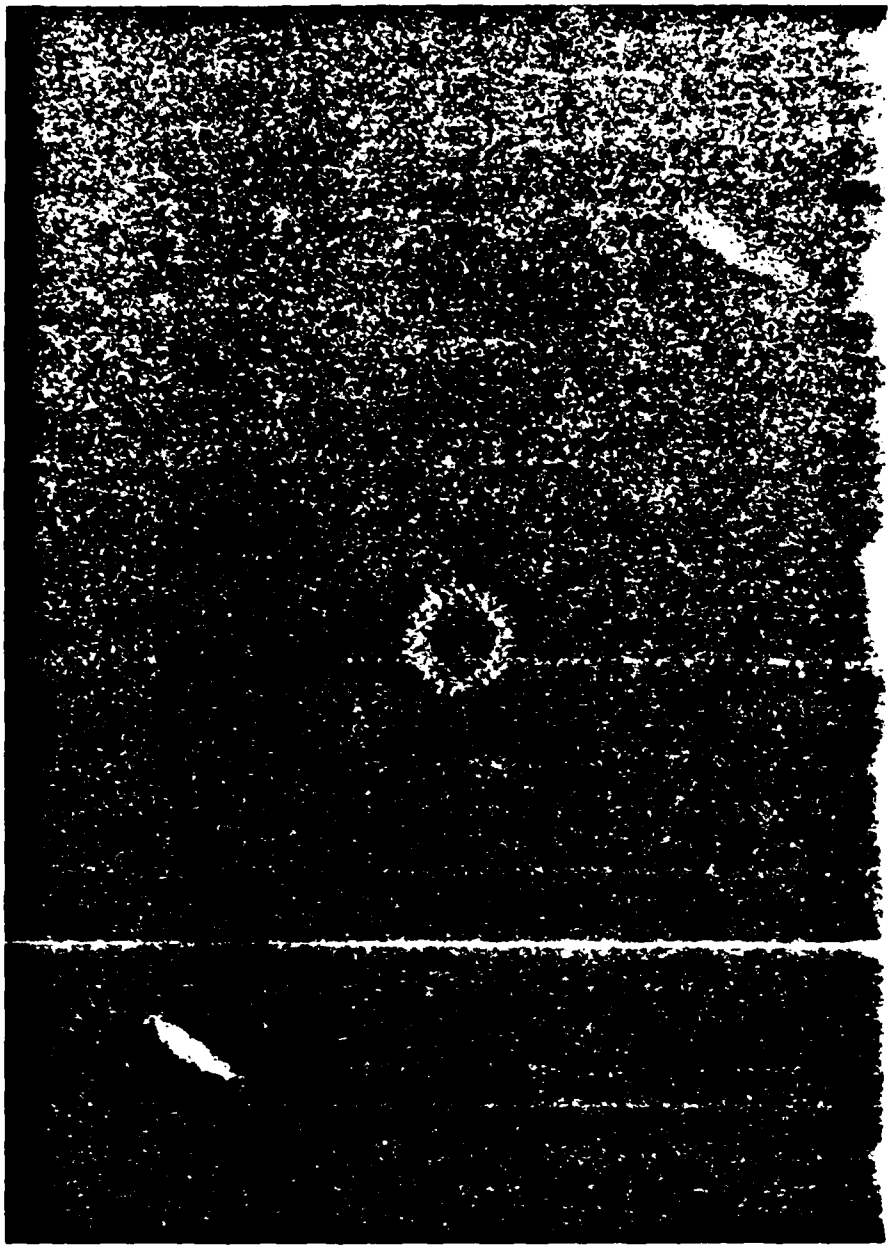

Figure 10. A fluorescent image of the electron ring as it strikes a uranium glass witness plate.

Within the last year we have tested two accelerator-gyrotron configurations. The first system, shown in Fig. 11, produced only low power at harmonics of the accelerator-driver frequency, which was not a gyrotron interaction. The beam bunched at harmonics of the x-band magnetron in the accelerator cavity and radiated coherently in the gyrotron cavity. However, the most serious problem with the first design was the breakdown of acceleration for beams with a modest value of current. For $I \lesssim 1mA$, the critically-coupled, linearly-polarized accelerator performed as expected, yielding electron kinetic energies greater than 100 keV. However, at higher values of current, the accelerator could not be excited by the magnetron and the result was a lack of electron acceleration. The situation can be explained in one of three ways: 1) the $B_\perp$ (waveguide) - $B_z$ (cavity) coupling broke down in the presence of a modest electron beam; 2) the high-Q cavity resonance shifted due to the extra energy dissipation mechanism; or 3) problems arose from the linearly polarized excitation.

Rather than continue wrestling with the first design, a second cavity system was built which was more faithful to the original design by Howard Jory.[5] Furthermore, the second design exploited the fact that since all modes are TE, longitudinal currents do not exist in the cavity walls. Therefore, the cavities need not be soldered together. The system consists of three pieces which are bolted together: an accelerator cavity, a gyrotron cavity, and a connecting drift tube. This has resulted in fabrication and reconfiguration simplicity.

The accelerator is a right cylindrical cavity. A diameter of 2.59 cm and a length of 2.16 cm were chosen so that the $TE_{111}$ resonant frequency of 9.2 GHz fell midway in the tuning band of the available magnetron sources. To couple between the dominant $TE_{10}$ half- height waveguide mode and the $TE_{111}$ cavity

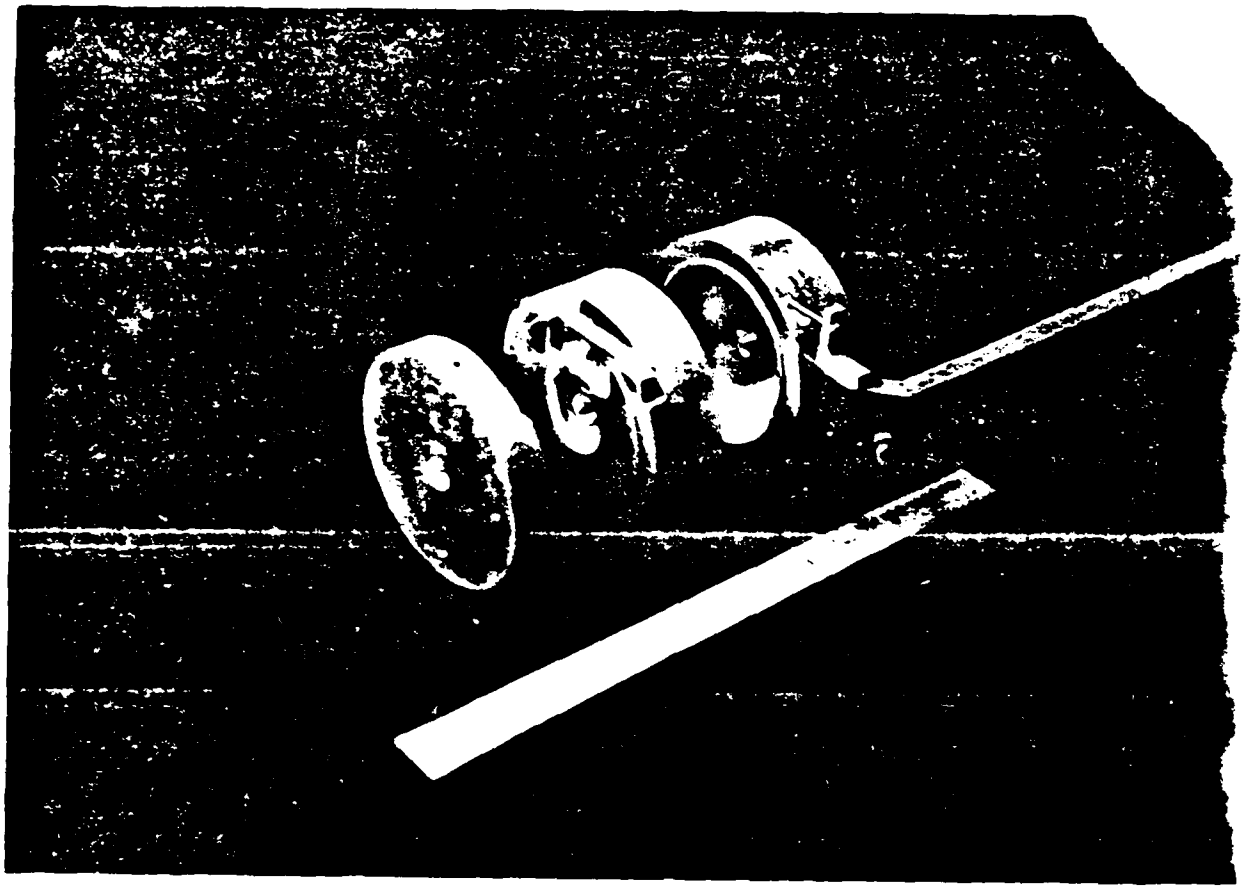

Figure 11. The accelerator and gyrotron cavities of the first tube design.

mode, a ¼" aperture near the center of the cavity was chosen to match the electric guide fields to the cavity $E_\phi$ fields. The waveguide-cavity system was designed to be overcoupled to compensate for magnetron frequency instability and cavity resonance "walk-off". A coupling coefficient of $\beta = 3$ was measured with a network analyzer. The circularly polarized $TE_{111}$ mode of the accelerator is now excited, i.e. we are coupling into the cavity through two apertures. The two waveguide lines which connect the cavity to the magic tee beam splitter are symmetric except for a small difference in the length of guide corresponding to $\lambda/4$. Therefore, the electric field at one coupling aperture is $90^o$ out of phase with respect to the other.

The high frequency interaction cavity has a diameter of 1.60 cm and a length of 5.08 cm. The radial component of the cavity electric field couples into WR-28 waveguide via a ¼" hole near the end of the cavity. The higher order longitudinal modes (e.g. $TE_{n12}$, $TE_{n13}$) are more heavily damped and are therefore less likely to oscillate. Figure 12 shows a schematic representation of the accelerator and high frequency cavity. A drift region with a diameter of 1.37 cm was chosen to allow propagation of a 500 keV beam into the interaction cavity from the accelerator. The drift tube is only 0.64 cm long in order to minimize early parasitic oscillations. Figure 13 displays actual cavity components--two accelerator cavities and four gyrotron cavities. The microwave tube is mounted on the vacuum interface flange in Fig. 14 and the entire system is schematically represented in Fig. 15.

The device has yielded 100 W level output at 26, 32, 38, and 45 GHz (third through sixth cyclotron harmonics), which represents approximately 1% energy conversion. The efficiency of electron energy conversion into the output wave as a function of beam current is shown in Fig. 16. The interaction saturates at relatively low beam currents due to the length of the cavity. The next cavity to be tested will be critically coupled, which will yield a factor of five

A. E-BEAM INPUT HOLE

B. ACCELERATOR CAVITY

C. DRIFT TUBE

D. INTERACTION CAVITY

E. E-BEAM EXIT HOLE

F. URANIUM GLASS BEAM IMAGER

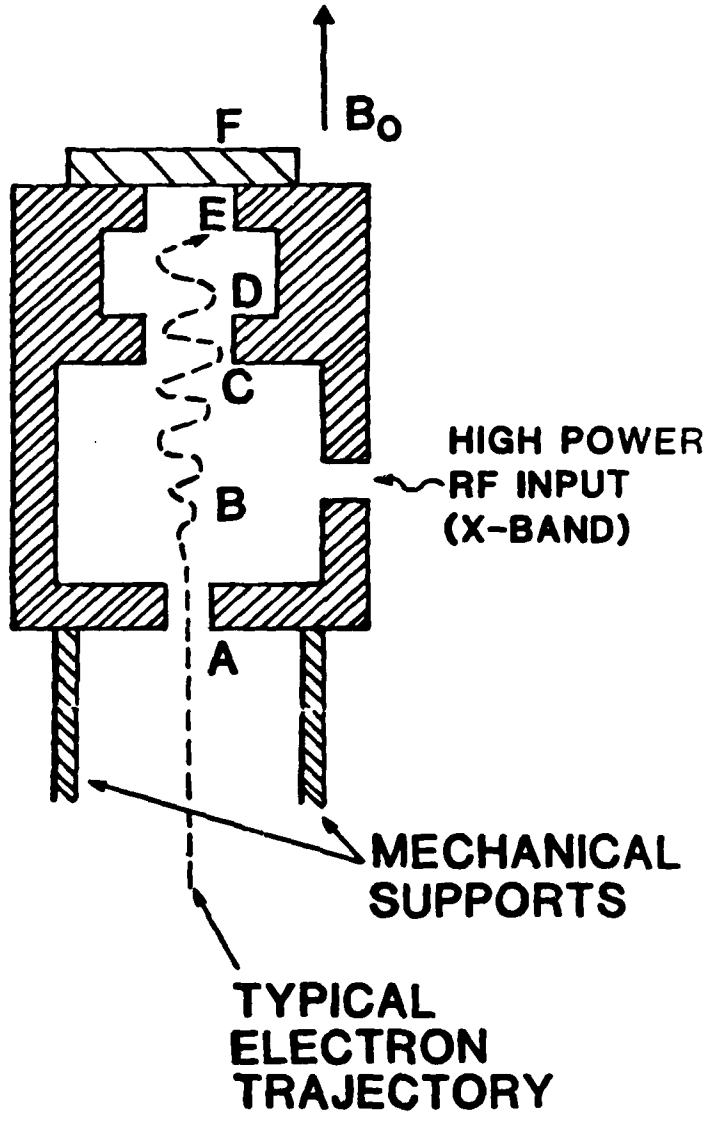


# ACCELERATOR & INTERACTION CAVITY

Figure 12. Schematic of the accelerator and gyrotron cavities.

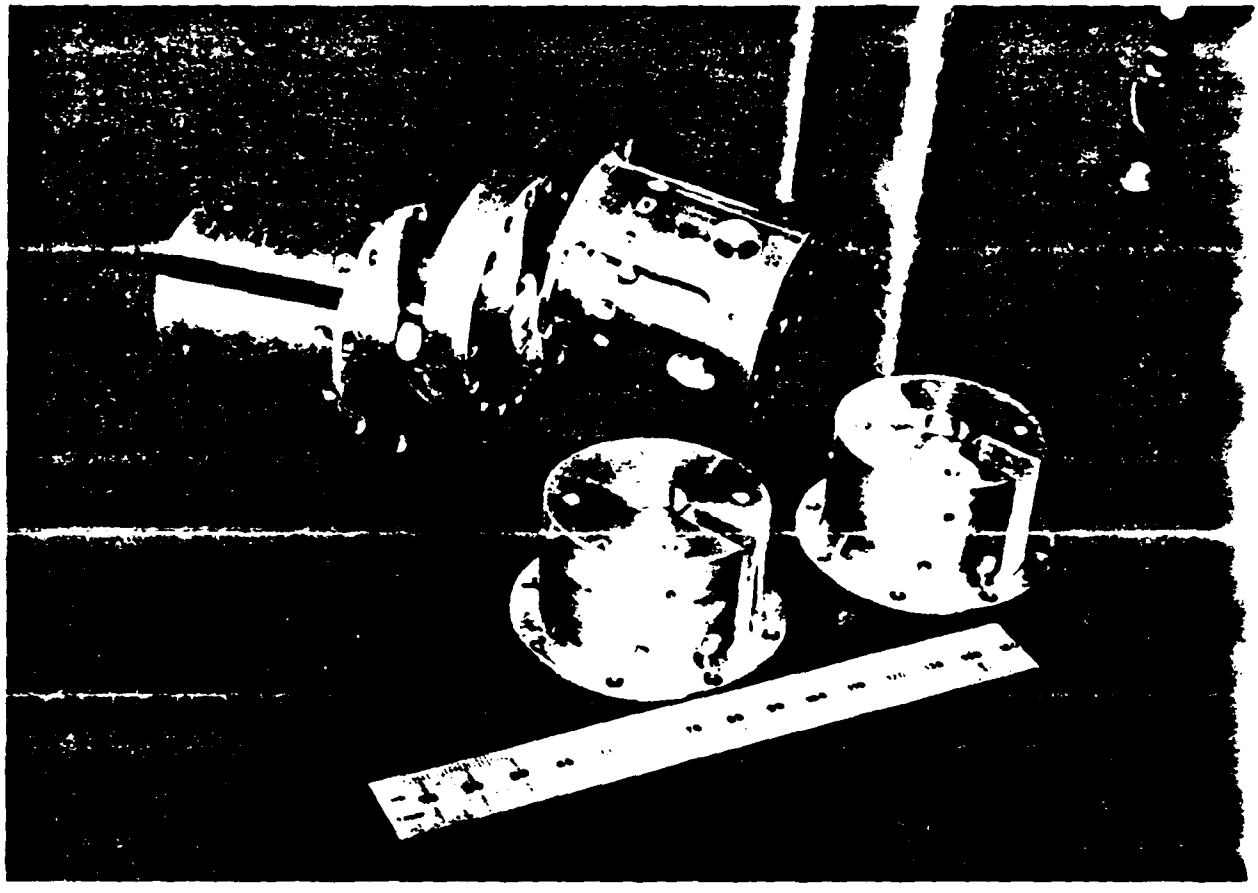

Figure 13. Sample accelerator and gyrotron cavities of the second tube design.

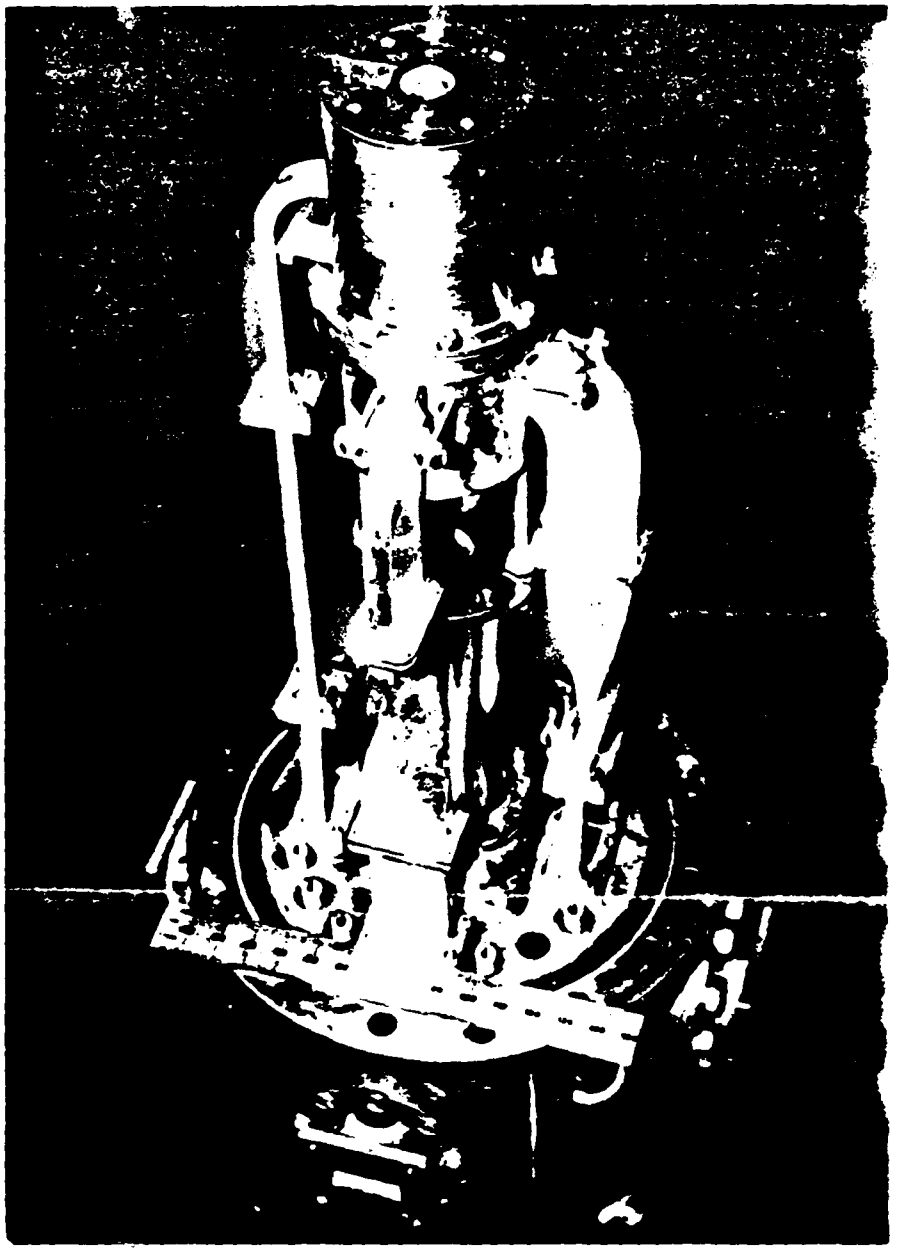

Figure 14. The harmonic gyrotron system mounted on the vacuum flange before it is bolted into the chamber.

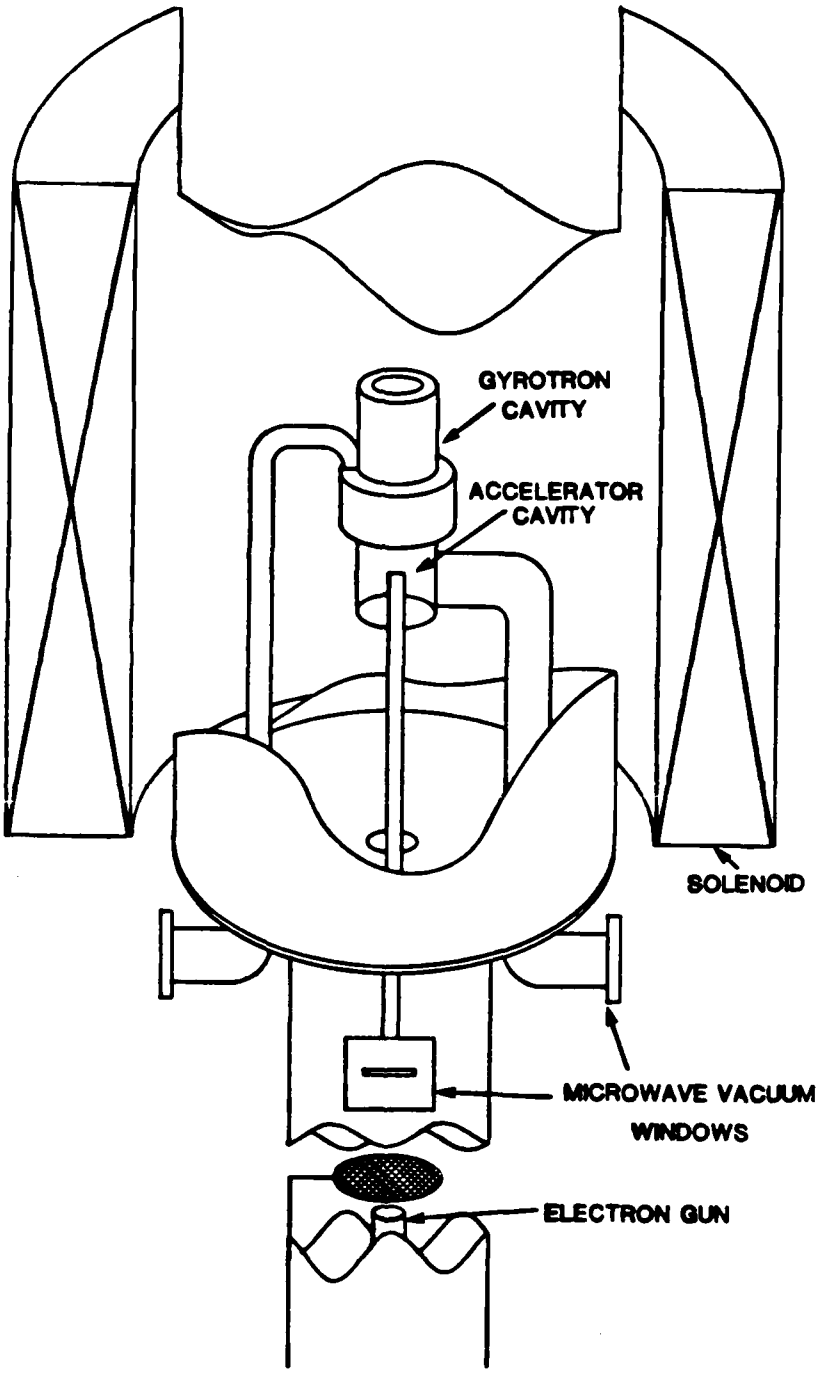


Figure 15. Schematic of the UCLA Cyclotron Harmonic Maser.

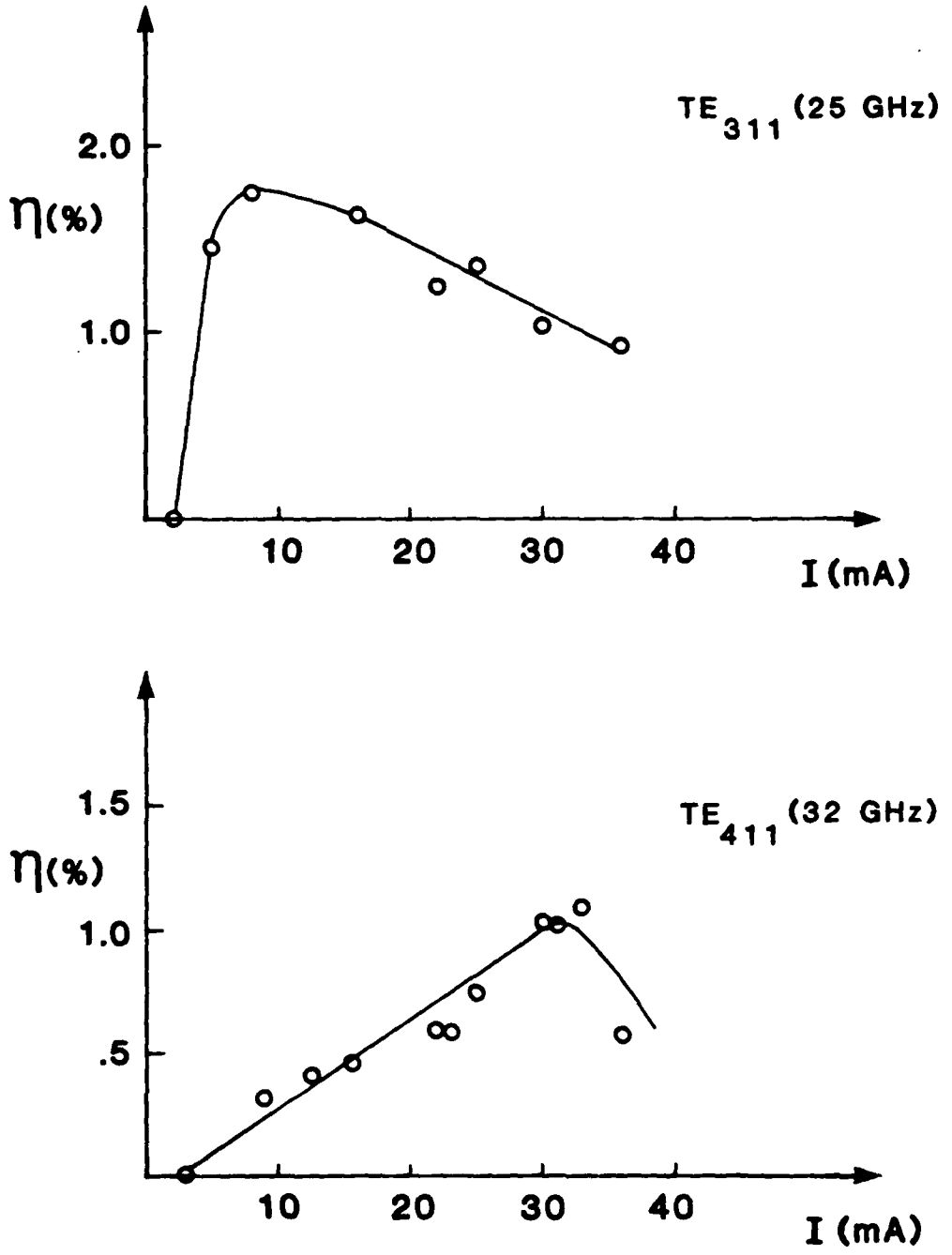


Figure 16. Experimental measurement of efficiency for the first harmonic gyrotron tube of the second design. Efficiency is defined as the ratio of rf output power to the input electron beam power.

increase in output power, and half the size, which should double the efficiency.

We have essentially verified the small-signal theory presented in the previous section by measuring the start-oscillation current. An evaluation of Eq. (8) for the parameters associated with the experiment--L/a = 6.35, a = .78 cm, $Q_L$ = 8000, $\beta$ = 0.10--yields $I_s$ = 1.5 mA for the $\gamma$ = 1.32, $TE_{411}$ interaction and 1.0 mA for the $\gamma$ = 1.21, $TE_{311}$ interaction, as shown in Fig. 17, in substantial agreement with the experimentally determined start oscillation current equal to 3.0 $\pm$ 1.0 mA and 2.0 $\pm$ 1.0 mA respectively, as shown in Fig. 18.

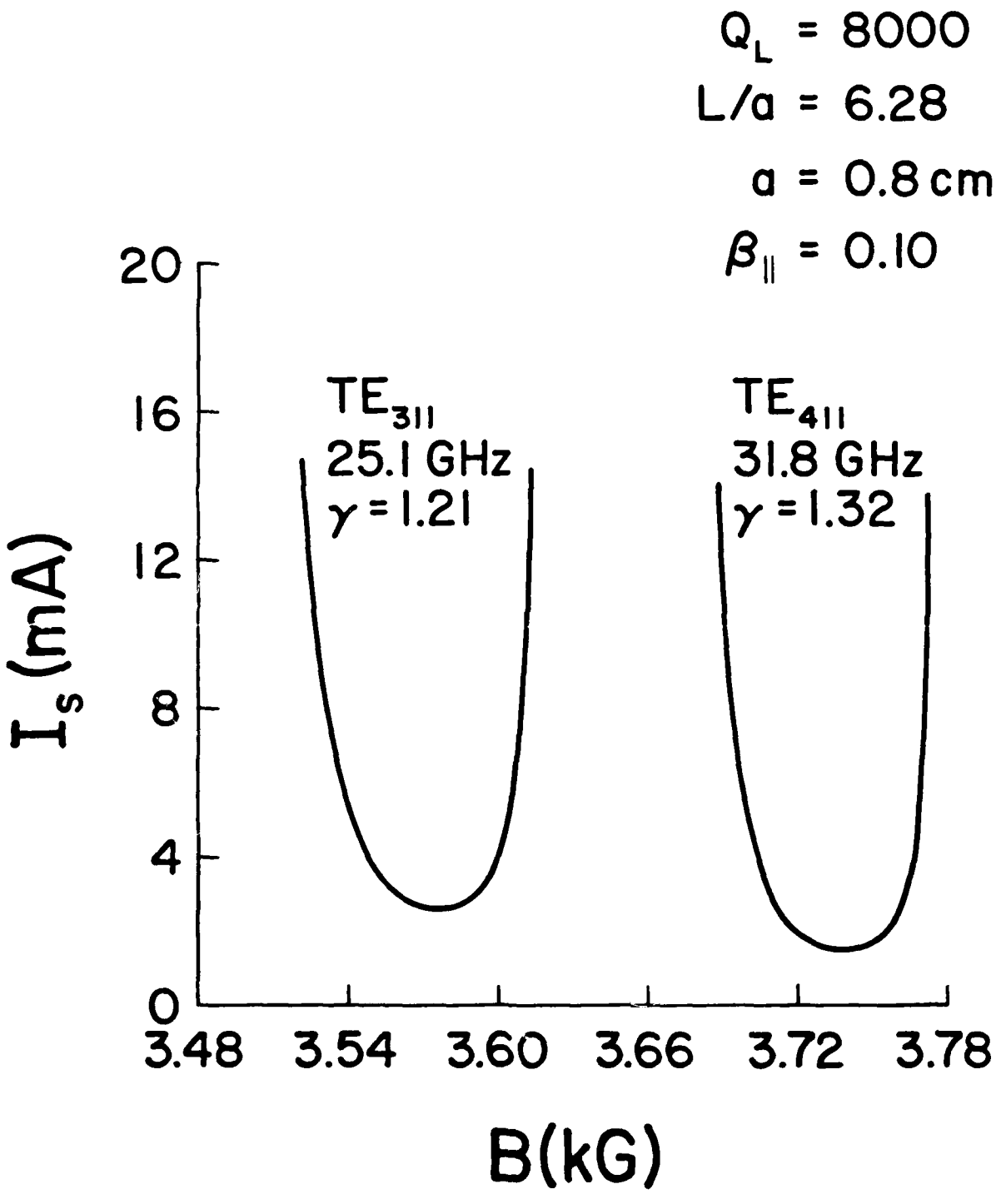


Figure 17. Theoretical plot of start-oscillation current for two harmonic interactions (n=3, 4) as a function of magnetic field for actual experimental parameters.

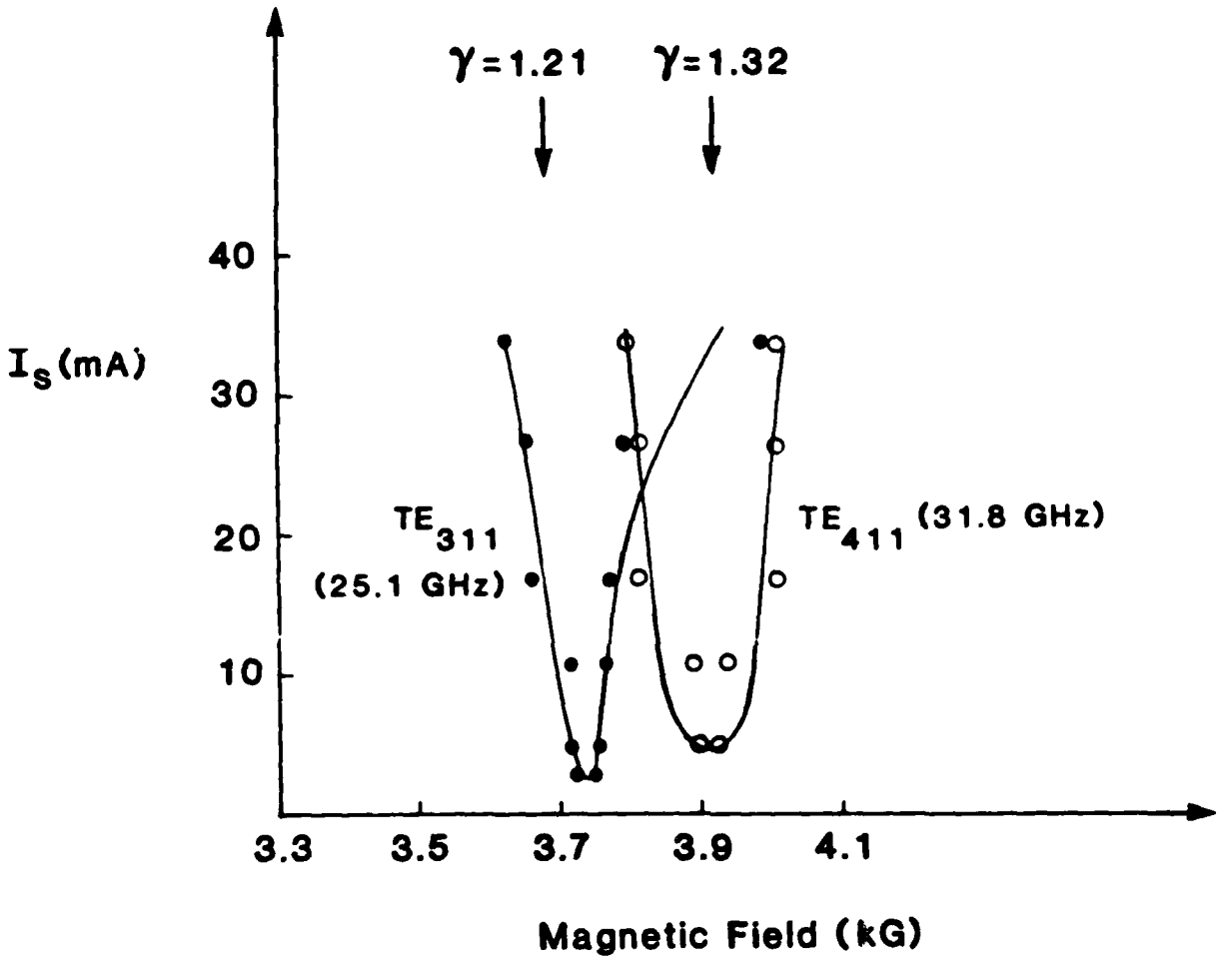


Figure 18. Experimental measurement of start-oscillation current for two harmonic interactions (n=3, 4) as a function of magnetic field.

## IV. REFERENCES


1. P. Sprangle and A. Drobot, IEEE Trans. Microwave Theory Tech. MTT-25, 528 (1977).

2. K.R. Chu. Digest--Sixth International Conference on Infrared and Millimeter Waves, "Recent Theoretical Developments in Gyrotron Research," Miami Beach, Florida (1981).

3. J.L. Hirshfield, I.B. Bernstein, and J.M. Wachtel, IEEE J. Quantum Electronics QE-1, 237 (1965).

4. K.R. Chu and J.L. Hirshfield, Phys. Fluids 1, 461 (1978).

5. H.R. Jory, "Investigation of Electronic Interaction with Optical Resonators for Microwave Generation and Amplification," U.S. Army Electronics Command Research and Development Technical Report ECOM-01873-F (1968).

## V. CONFERENCES AND PUBLICATIONS

### CONFERENCES

1. The Sixth International Conference on Infrared and Millimeter Waves, Sponsored by the IEEE Microwave Theory and Techniques Society, Miami Beach, Florida, Dec. 7-12, 1981.

2. USA-Japan Workshop on Sub-Millimeter Diagnostics Techniques, Institute of Plasma Physics, Nagoya, Japan, Jan. 18-21, 1982.

### PUBLICATIONS

1. F. Allen, Y. Bae, S.S. Iyer, C. Jou, A. Kupiszewski, N. Lee, N.C. Luhmann, Jr. D.B. McDermott, R.A. Metzer, D.S. Pan, W.A. Peebles, D. Rutledge, D. Umstadter, Y. Xu, and C.C. Yang, "Current Millimeter and Submillimeter Wave Source Development at UCLA," USA-Japan Workshop on Submillimeter Diagnostic Techniques, Nagoya, Japan, Jan. 18-21, 1982.

2. D.B. McDermott, N.C. Luhmann, Jr., A. Kupiszewski, and H.R. Jory, "Small-Signal Theory of a Large Orbit Electron Cyclotron Harmonic Maser," submitted to Phys. Fluids.

UNCLASSIFIED

SECURITY CLASSIFICATION OF THIS PAGE (When Data Entered)

| REPORT DOCUMENTATION PAGE | READ INSTRUCTIONS BEFORE COMPLETING FORM |
|---|---|
| 1. REPORT NUMBER AFOSR-TR- 82-0866 | 2. GOVT ACCESSION NO. AD-A120 318 |
| 3. RECIPIENT'S CATALOG NUMBER | |
| 4. TITLE (and Subtitle) COMPACT MILLIMETER WAVE CYCLOTRON RESONANCE MASER | 5. TYPE OF REPORT & PERIOD COVERED PROGRESS REPORT JUNE 15, 1981-JUNE 15, 1982 |
| 6. PERFORMING ORG. REPORT NUMBER ENG- 82-65 | |
| 7. AUTHOR(s) N.C. LUHMANN, JR. D.B. MCDERMOTT | 8. CONTRACT OR GRANT NUMBER(s) AFOSR 81-0200 |
| 9. PERFORMING ORGANIZATION NAME AND ADDRESS DEPARTMENT OF ELECTRICAL ENGINEERING 7702 BOELTER HALL UCLA, CA 90024 | 10. PROGRAM ELEMENT, PROJECT, TASK AREA & WORK UNIT NUMBERS 61102F 2301/A8 |
| 11. CONTROLLING OFFICE NAME AND ADDRESS AFOSR/NP Building 410 Bolling AFB DC 20332 | 12. REPORT DATE AUGUST 1982 |
| | 13. NUMBER OF PAGES 35 |
| 14. MONITORING AGENCY NAME & ADDRESS(if different from Controlling Office) | 15. SECURITY CLASS. (of this report) UNCLASSIFIED |
| | 15a. DECLASSIFICATION/DOWNGRADING SCHEDULE |

16. DISTRIBUTION STATEMENT (of this Report)

Approved for public release; distribution unlimited

17. DISTRIBUTION STATEMENT (of the abstract entered in Block 20, if different from Report)

18. SUPPLEMENTARY NOTES

19. KEY WORDS (Continue on reverse side if necessary and identify by block number)

CYCLOTRON HARMONIC MASER, RF ACCELERATOR, GYROTRON, CONVERSION EFFICIENCY, MAGNETIC FIELD TAPERING, SMALL-SIGNAL THEORY, START-OSCILLATION CURRENT.

20. ABSTRACT (Continue on reverse side if necessary and identify by block number)

The initial results of the cyclotron harmonic resonance maser have been extremely encouraging. Using only 50 kW of the 200 kW available from our X-band magnetron, the rf accelerator has produced 100 mA, 100-250 keV beams. Furthermore, moderate power sub-cm output has been produced. Our second gyrotron cavity, which was designed to be excited by ~ 150 keV beams, has yielded ~ 100 W at 26-46 GHz (3rd - 6th cyclotron harmonics), corresponding to 1% electron to output wave conversion efficiency. This cavity was designed

DD FORM 1 JAN 73 1473

82 UNCLASSIFIED 182

SECURITY CLASSIFICATION OF THIS PAGE (When Data Entered)

Block 20 (cont.)

undercoupled for easy start-oscillation. Therefore, the efficiency of electron energy into cavity wave power was on the order of 5%. The next cavity to be tested is critically coupled for higher power operation.

Our theoretical activities have also been productive. We have developed a theoretical description of the large-orbit cyclotron harmonic maser which yields encouraging values for device efficiency. Efficiencies as high as 8% have been predicted at millimeter-wavelength operation with a uniform magnetic field. By properly tapering the magnetic field so that the gyrofrequency remains approximately constant as the electrons may be increased to 16%. In addition, a small-signal theory of the harmonic gyrotron has been developed which yields the value for the start-oscillation current. This theory has already been verified by experimental measurements. An important result is, though a shorter cavity will have a higher peak efficiency, a longer cavity requires less beam current for oscillation.

USA - JAPAN WORKSHOP

ON SUBMILLIMETER DIAGNOSTIC TECHNIQUES

January 18-21, 1982

Nagoya, Japan

# CURRENT MILLIMETER AND SUBMILLIMETER WAVE SOURCE DEVELOPMENT EFFORTS AT UCLA

F. Allen, Y. Bae, S. S. Iyer*, C. Jou, A. Kupiszewski

N. Lee, N. C. Luhmann, Jr., D. B. McDermott, R. A. Metzer,

D. S. Pan, W. A. Peebles, D. Rutledge**, D. Umstadter, Y. Xu and C. C. Yang

University of California

Los Angeles, California

A brief overview of the current UCLA source development effort is given.

*Permenent Address: IBM Watson Research Center 8-258
Yorktown Hts., N.Y. 10598

**Permenent Address: California Institute of Techology
Pasadena, California

# 1. INTRODUCTION

There is currently a critical need for efficient sources in the millimeter and submillimeter wave region. These include cw milliwatt level local oscillators for use in heterodyne receivers as well as $1\text{-}10^6$W level sources for applications such as plasma diagnostics, secure c mmunications and imaging radars. There is presently a large experimental and theoretical effort by various groups in the UCLA Electrical Engineering Department aimed at addressing this need.

Compact relativistic cyclotron resonance masers are being investigated for operation in the 90-1000 GHz region. Silicon molecular beam epitaxy (MBE) is being used to fabricate solid state sources such as TUNNETT structures, IMPATT's and MOS varactor sub-millimeter wave doublers. In parallel, there is an active theoretical program involved in the design and modeling of these devices. Particular emphasis is being placed on studying the high frequency limitations of transit-time diodes and novel variations of them with the goal of improving their power capabilities. Finally, the ring resonator optically pumped far-infrared laser is being studied. The goal is to produce single mode output at the megawatt level.

SUBMITTED TO THE PHYSICS OF FLUIDS

# SMALL-SIGNAL THEORY OF A LARGE ORBIT ELECTRON CYCLOTRON HARMONIC MASER

D.B. McDermott, N.C. Luhmann, Jr. and A. Kupiszewski

University of California
Los Angeles, CA 90024

and

H.R. Jory

Varian Associates
Palo Alto, CA 94303

The small-signal theory of a harmonic gyrotron is presented for the case of axis-encircling electron orbits. The beam current required for oscillation is found to be highly dependent on the electron energy. Gyrotron cavities operating on this principle at very high harmonic numbers ($n \approx 10$) and high frequency in weak magnetic fields are well matched to low current, moderate energy, rf-accelerated electron beams ($\approx 50$ mA, $\approx 250$ keV), resulting in compact submillimeter wave systems.


DATE
ILME